Non-invasive optical interferometry for the assessment of biofilm growth in the middle ear

Cac T. Nguyen,[1,2] Haohua Tu,[1] Eric J. Chaney,[1] Charles N. Stewart,[4] and Stephen A. Boppart[1,2,3,*]

[1]*Beckman Institute for Advanced Science and Technology, University of Illinois at Urbana-Champaign, 405 North Mathews Avenue, Urbana, IL, 61801, USA*
[2]*Department of Electrical and Computer Engineering, University of Illinois at Urbana-Champaign, 405 North Mathews Avenue, Urbana, IL, 61801, USA*
[3]*Department of Bioengineering, Department of Medicine University of Illinois at Urbana-Champaign, 405 North Mathews Avenue, Urbana, IL, 61801, USA*
[4]*Blue Highway, LLC, Welch Allyn, Inc., 2-212 Center for Science & Technology, Syracuse, NY 13244, USA*
**boppart@illinois.edu*

Abstract: Otitis media (OM) is the most common illness in children in the United States. Three-fourths of children under the age of three have OM at least once. Children with chronic OM, including OM with effusion and recurrent OM, will often have conductive hearing loss and communication difficulties, and need surgical treatment. Recent clinical studies provide evidence that almost all chronic OM cases are accompanied by a bacterial biofilm behind the tympanic membrane (eardrum) and within the middle ear. Biofilms are typically very thin, and cannot be recognized using a regular otoscope. Here we demonstrate how optical low coherence interferometry (LCI) noninvasively depth-ranges into the middle ear to detect and quantify biofilm microstructure. A portable diagnostic system integrating LCI with a standard video otoscope was constructed and used to detect and quantify the presence of biofilms in a newly-developed pre-clinical animal model for this condition. Using a novel classification algorithm for acquired LCI data, the system identified the presence of a biofilm with 86% sensitivity and 90% specificity, compared to histological findings. This new information on the presence of a biofilm, its structure, and its response to antibiotic treatment, will not only provide better understanding of fundamental principles that govern biofilm formation, growth, and eradication, but may also provide much needed clinical data to direct and monitor protocols for the successful management of otitis media.

OCIS codes: (170.4500) Optical coherence tomography; (170.4940) Otolaryngology.

References and links

1. J. O. Klein, "Otitis media," Clin. Infect. Dis. **19**(5), 823–833 (1994).
2. J. E. Roberts, R. M. Rosenfeld, and S. A. Zeisel, "Otitis media and speech and language: a meta-analysis of prospective studies," Pediatrics **113**(3), e238–e248 (2004).
3. S. M. Pransky, "Surgical strategies for otitis media," J. Otolaryngol. **27**(Suppl 2), 37–42 (1998).
4. J. Froom, L. Culpepper, M. Jacobs, R. A. DeMelker, L. A. Green, L. van Buchem, P. Grob, and T. Heeren, "Antimicrobials for acute otitis media? A review from the International Primary Care Network," BMJ **315**(7100), 98–102 (1997).
5. P. Shekelle, G. Takata, L. S. Chan, R. Mangione-Smith, P. M. Corley, T. Morphew, and S. Morton, "Diagnosis, natural history, and late effects of otitis media with effusion," Agency for Healthcare Research and Quality Publication No. 03–E023 (2003).
6. P. K. Harris, K. M. Hutchinson, and J. Moravec, "The use of tympanometry and pneumatic otoscopy for predicting middle ear disease," Am. J. Audiol. **14**(1), 3–13 (2005).
7. L. Hall-Stoodley, F. Z. Hu, A. Gieseke, L. Nistico, D. Nguyen, J. Hayes, M. Forbes, D. P. Greenberg, B. Dice, A. Burrows, P. A. Wackym, P. Stoodley, J. C. Post, G. D. Ehrlich, and J. E. Kerschner, "Direct detection of

#132874 - $15.00 USD Received 4 Aug 2010; revised 4 Oct 2010; accepted 4 Oct 2010; published 7 Oct 2010

bacterial biofilms on the middle-ear mucosa of children with chronic otitis media," JAMA **296**(2), 202–211 (2006).
8. J. E. Dohar, P. A. Hebda, R. Veeh, M. Awad, J. W. Costerton, J. Hayes, and G. D. Ehrlich, "Mucosal biofilm formation on middle-ear mucosa in a nonhuman primate model of chronic suppurative otitis media," Laryngoscope **115**(8), 1469–1472 (2005).
9. M. Allegrucci, F. Z. Hu, K. Shen, J. Hayes, G. D. Ehrlich, J. C. Post, and K. Sauer, "Phenotypic characterization of *Streptococcus pneumoniae* biofilm development," J. Bacteriol. **188**(7), 2325–2335 (2006).
10. C. Potera, "Forging a link between biofilms and disease," Science **283**(5409), 1837–1839, 1839 (1999).
11. J. W. Costerton, P. S. Stewart, and E. P. Greenberg, "Bacterial biofilms: a common cause of persistent infections," Science **284**(5418), 1318–1322 (1999).
12. W. Drexler, and J. Fujimoto, *Optical Coherence Tomography: Technology and Applications*, (Springer, New York, 2008).
13. A. M. Zysk, F. T. Nguyen, A. L. Oldenburg, D. L. Marks, and S. A. Boppart, "Optical coherence tomography: a review of clinical development from bench to bedside," J. Biomed. Opt. **12**(5), 051403 (2007).
14. C. Pitris, K. T. Saunders, J. G. Fujimoto, and M. E. Brezinski, "High-resolution imaging of the middle ear with optical coherence tomography: a feasibility study," Arch. Otolaryngol. Head Neck Surg. **127**(6), 637–642 (2001).
15. H. R. Djalilian, J. Ridgway, M. Tam, A. Sepehr, Z. Chen, and B. J. Wong, "Imaging the human tympanic membrane using optical coherence tomography *in vivo*," Otol. Neurotol. **29**(8), 1091–1094 (2008).
16. C. Xi, D. L. Marks, S. Schlachter, W. Luo, and S. A. Boppart, "High-resolution three-dimensional imaging of biofilm development using optical coherence tomography," J. Biomed. Opt. **11**(3), 034001 (2006).
17. W. Jung, D. T. McCormick, Y. C. Ahn, A. Sepehr, M. Brenner, B. Wong, N. C. Tien, and Z. Chen, "*In vivo* three-dimensional spectral domain endoscopic optical coherence tomography using a microelectromechanical system mirror," Opt. Lett. **32**(22), 3239–3241 (2007).
18. D. T. McCormick, W. Jung, Y. C. Ahn, V. Milanović, Z. Chen, and N. C. Tien, "A MEMS based optical coherence tomography imaging system and optical biopsy probes for real-time, high resolution *in-vivo* and *in-vitro* 2-D or 3-D imaging," in *Proceedings of 2006 IEEE/LEOS International Conference on Optical MEMS and their Applications* (August 2006) pp. 2.
19. A. M. Zysk, and S. A. Boppart, "Computational methods for analysis of human breast tumor tissue in optical coherence tomography images," J. Biomed. Opt. **11**(5), 054015 (2006).
20. B. D. Goldberg, N. V. Iftimia, J. E. Bressner, M. B. Pitman, E. Halpern, B. E. Bouma, and G. J. Tearney, "Automated algorithm for differentiation of human breast tissue using low coherence interferometry for fine needle aspiration biopsy guidance," J. Biomed. Opt. **13**(1), 014014 (2008).
21. E. L. Tonnaer, E. A. Sanders, and J. H. Curfs, "Bacterial otitis media: a new non-invasive rat model," Vaccine **21**(31), 4539–4544 (2003).
22. O. B. Piltcher, J. D. Swarts, K. Magnuson, C. M. Alper, W. J. Doyle, and P. A. Hebda, "A rat model of otitis media with effusion caused by eustachian tube obstruction with and without *S. pneumoniae* infection: Methods and disease course," Otolaryngol. Head Neck Surg. **126**(5), 490–498 (2002).
23. M. Hoa, M. Syamal, L. Sachdeva, R. Berk, and J. Coticchia, "Demonstration of nasopharyngeal and middle ear mucosal biofilms in an animal model of acute otitis media," Ann. Otol. Rhinol. Laryngol. **118**(4), 292–298 (2009).
24. W. Jung, W. Benalcazar, U. Shamar, A. Ahmad, H. Tu, and S. A. Boppart, "Numerical analysis of GRIN lens-based OCT imaging probes," J. Biomed. Opt. under review.
25. J. Canny, "A computational approach to edge detection," IEEE Trans. Pattern Anal. Mach. Intell. **8**(6), 679–698 (1986).
26. R. Deriche, "Using Canny's criteria to derive a recursively implemented optimal edge detector," Int. J. Comput. Vis. **1**(2), 167–187 (1987).
27. D. J. Lim, "Structure and function of the tympanic membrane: a review," Acta Otorhinolaryngol. Belg. **49**(2), 101–115 (1995).

1. Introduction

1.1. Otitis media and biofilm

Otitis media (OM) is a middle ear infection between the tympanic membrane (TM) and the inner ear. An ear infection occurs when bacteria grow in the middle ear, causing the accumulation of fluid, swelling, and inflammation. Young children often acquire ear infections after colds, food allergies, or respiratory infections. Middle ear infections occurs in about 75% of children by the age of three, and are the most common cause of visits to a physician at this age [1,2]. Classification of ear infections is based on symptoms, duration, and physical diagnosis. The most common type is acute otitis media (AOM), which is a rapid infection with one or more symptoms such as otalgia, fever, and irritability. In this case, physicians often find an abnormal appearing tympanic membrane with pneumatic otoscopy, including bulging, opacity, effusion, and decreased mobility.

#132874 - $15.00 USD Received 4 Aug 2010; revised 4 Oct 2010; accepted 4 Oct 2010; published 7 Oct 2010

Otitis media can be a recurrent disease and more than one third of children under the age of seven experience at least six recurrent episodes of AOM. Middle ear effusions often follow AOM, producing chronic infection. Even though chronic infection can cause long-term or permanent damage to the ear, there may be fewer pronounced signs or symptoms of infection than in AOM, which may cause the infection to go unnoticed and untreated for an extended period of time. Chronic OM can often cause tissue hardening, pus-like drainage, damage to the mastoid bone, and damage to the bones in the middle ear involved in hearing [2,3]. Therefore, the disease often causes hearing loss and communication impairment, especially in small children who are in the process of learning to speak.

Acute otitis media may clear in one to two weeks without treatment, or may need to be treated with antibiotics. About 50% of antibiotic prescriptions for children less than three years old are given for ear infections. However, in the case of chronic OM, antibiotics may no longer be helpful, and placing a tympanostomy tube in the TM is strongly recommended. The tympanostomy tube helps drain the fluid accumulating behind the TM directly into the outer ear canal. This surgery is also the most common surgical procedure for young children [2,3].

Given the associated morbidity and costs of this disease, it is very important not only to accurately diagnose middle ear infections in order to determine the most effective treatment, but also to monitor the regression or progression of this disease in a quantitative manner. Overuse and misuse of antibiotics in OM haves contributed to resistant bacteria, further complicating the management of this disease [4]. The diagnostic challenge is the difficulty in discriminating acute OM from chronic OM, and the antibiotic treatment response, using a standard otoscope. This challenge exists even for physicians experienced in visually investigating the various colors and shapes of the TM, and the presence and characterization of any middle ear fluid or effusion.

Currently, chronic OM is diagnosed by several methods. Standard otoscopy is most frequently used, however the signs of OM are not always apparent. Therefore, the accuracy of standard otoscopy is limited with a sensitivity and specificity of 74% and 60%, respectively [5]. Other currently available diagnostic methods such as pneumatic otoscopy and tympanometry can yield slightly higher sensitivities and specificities (70-90%) under ideal conditions, compared to standard otoscopy [5,6]. However, both pneumatic otoscopy and tympanometry still have technical problems with obtaining a good seal within the patient's ear canal, complicating the measurement. Accurate measurements require that the correct size of ear speculum be used and depend heavily on patient cooperation. Other factors like cerumen or pressure level also have an effect on the measurement accuracy. Therefore, a combination of the three methods: otoscopy, pneumatic otoscopy, and tympanometry, if necessary, is now recommended for the diagnosis of chronic OM [5,6]. Furthermore, these methods are helpful in detecting effusions in chronic OM, but remain limited in their ability to qualitatively or quantitatively track changes in the effusion during treatment.

Recent clinical studies have shown strong evidence that there is a one-to-one correspondence between chronic OM and the presence of a bacterial biofilm behind the TM. Mucosal biofilms were visualized by confocal laser scanning microscopy in 46 out of 52 middle ear mucosal specimens from 26 patients undergoing tympanostomy tube placement for chronic OM [7]. There are also observations of biofilm formation in induced chronic OM in animal models such as the chinchilla and monkey [8]. It has been shown that the pathogenic bacteria, *Pseudomonas aeruginosa*, which exists in all infected middle ear cultures, forms a biofilm in the middle ear.

In general, biofilms are a habitat for complex multi-species micro-organisms (e.g. bacteria, fungi, viruses, etc) that grow communally in adhesive self-forming biopolymers. Within biofilms, microbes are protected from harsh environments, including antibiotic or biocide treatments. Biofilm structures were recently found to be highly heterogeneous in composition and architecture including cell distribution, cell aggregation, structural voids, and fluid channels. The presence of a middle-ear biofilm is now considered a reservoir for bacteria and

#132874 - $15.00 USD Received 4 Aug 2010; revised 4 Oct 2010; accepted 4 Oct 2010; published 7 Oct 2010

a cause of OM, explaining why antibiotics have not been optimally effective for chronic OM [9–11].

1.2. Low coherence interferometry technique

Low coherence interferometry is an optical ranging technique that is capable of measuring one-dimensional depth-resolved tissue structure. To perform LCI, low coherence light is generated from a broadband optical source and split by a beam splitter or fiber-optic coupler into two beams which are sent to sample and reference arms of the interferometer. The reference arm contains a stationary mirror, while the sample arm contains beam-delivery optics to direct the beam toward the sample. The interference of the two back-reflected or scattered beams is captured by a linear photodetector array and processed by a computer to describe the depth-resolved optical scattering properties of the tissue [Fig. 1(a)]. The broadband, near-infrared light used in LCI allows for axial resolutions of up to 2-3 μm, and penetration depths of up to 2-3 mm in highly-scattering tissues. The spatial variations in the optical backscattered signal are used to describe the microstructures of the tissues. With additional transverse (lateral) scanning mechanisms and by assembling adjacent depth scans, optical coherence tomography (OCT) images can be generated, which represent cross-sectional images of tissue [12,13].

Imaging of the middle ear using the LCI/OCT technique has been demonstrated by several research groups [14,15]. With *ex vivo* OCT imaging, all micro-structures of the middle ear such as the TM, malleus, incus, chodra tympani nerve, and tendon of the tensor tympani muscle can be readily identified. With high resolution, LCI/OCT is also capable of imaging the micro-structure of biofilms, including the dynamics of biofilm formation in a laboratory flow-cell experiment where the three-dimensional structure was visualized over time [16].

The use of LCI or OCT for middle ear assessment and imaging offers several advantages. First, these techniques have the potential to non-invasively detect and quantitatively assess the presence of a biofilm behind the TM, while standard otoscopy or ultrasound imaging cannot. Second, while both LCI and OCT can provide new useful information, LCI is faster and more compact, with fewer requirements for mechanical scanning compared to OCT. Small disposable fibers mounted in ear specula can be used to perform LCI, instead of complex micro-mechanical scanning systems (MEMs). Even though MEMs-based scanners would make OCT imaging of the ear possible [17,18], the LCI technique is more suitable for portable systems. Finally, the integration of the LCI system with otoscopy enables a simple, low-cost, and non-invasive solution for providing new and quantitative information on the middle ear, particularly for detecting, assessing, and monitoring the middle ear for a biofilm, and their role in the treatment of OM.

In previous studies, LCI data have been demonstrated to be efficient for classifying human breast tissue [19,20]. Data from the middle ear acquired by an LCI system (i.e., axial scans) can be used to quantitatively characterize middle ear structure and classify OM status. In general, acute OM and chronic OM can be classified by the absence or presence of a bacterial biofilm, respectively. Biofilms and the TM are visualized in LCI data by various scattering layers. Here, we present a method to analyze these layers from each axial scan using three different parameters: thickness of TM with or without a biofilm layer, intensity of optical backscatter, and optical attenuation through structures. The statistical result of axial scan classification can be used to determine the likelihood of a biofilm being present, and can provide the physician with a quantitative parameter for OM diagnosis.

For this study, an integrated LCI-otoscope was constructed to acquire middle-ear data from a new rat model for chronic middle-ear biofilms. A new classification algorithm for the LCI data was also developed to statistically demonstrate, using histological observations as the gold standard, the identification of biofilms in the middle ear.

#132874 - $15.00 USD Received 4 Aug 2010; revised 4 Oct 2010; accepted 4 Oct 2010; published 7 Oct 2010

2. Materials and methods

2.1. Animal model and biofilm induction

Demonstration of our LCI system and methodology was first implemented in a new rat OM model that we developed explicitly for this research. All animal studies were conducted under a protocol approved by the Institutional Animal Care and Use Committee (IACUC) at the University of Illinois at Urbana-Champaign. *Streptococcus pneumoniae* biofilms were induced in Sprague-Dawley rats (Harlan, Indianapolis, IN) using a minimally-invasive technique involving nasal cannula delivery and pressurization to deliver bacteria to the middle ear via the Eustachian tube. The rat has previously been widely used as a model for OM, by introducing bacteria through a perforated TM or bulla. While there have been many reported methods for inducing OM in different animal models [21,22], only one recent report has described a protocol for inducing middle-ear biofilms in animals [23].

To induce middle-ear biofilms, rats were inoculated biweekly and checked daily for the development of OM. Rats were first anesthetized using a subcutaneous injection of Carprofen (5mg/kg) followed by an intraperitoneal injection of ketamine (100mg/kg) and xylazine (10mg/kg). A 30 µl volume of *Streptococcus pneumoniae* bacteria in a saline/1% methylcellulose solution at a concentration of 1 x 10^{10} CFU/ml was delivered into the left nasal cavity via a Teflon cannula. The rats were immediately transferred to a pressure chamber in which the air pressure was gradually raised to 50 kPa over 5 minutes, held at 50 kPa for 5 minutes, and then gradually reduced back to atmospheric pressure over 5 minutes.

In the first group of five animals, four of them were inoculated and one was used as a control. The inoculation was initially performed once a week. After 5 weeks without observing signs or symptoms of OM, the animal protocol was modified and bacterial inoculations were done biweekly instead of weekly. Since biofilms were expected to develop after several recurrent OMs, a second animal group of four additional rats was inoculated in order to have more animals with OM.

The increased chamber pressure drove the *Pneumococcal* inoculation bolus into the middle ear, resulting in acute and chronic middle ear infections and growth of biofilms over a total period of 7 months. At various time points, *in vivo* video otoscopy images and LCI data from the TMs of these animals were collected. Normal conditions, acute and chronic infections, and middle ear biofilms were observed. All of the TMs were dissected out for secondary *ex vivo* OCT imaging, and were subsequently fixed and embedded in paraffin for histological sectioning and comparative examination.

2.2 Instrumentation

The integrated otoscopy system was comprised of three main components: the LCI core, the LCI probe, and a standard video otoscope. A laptop was used to run custom software to control the system and process, analyze, and display both the video otoscope and LCI data. This system is compact, portable, and convenient for use in outpatient clinic settings [Fig. 1(b)].

LCI CORE: A super luminescence diode (SLD) (Pilot-2, Superlum, Ireland) was used as the low-coherence light source of the LCI system. This SLD has a center wavelength of 940 nm and a bandwidth of 70 nm, enabling an axial resolution of ~4.5 µm in tissue. The interference fringes generated by back reflections from the sample and reference arms were detected by a line-scan camera (P2-22 2K40, Dalsa, Inc.) with 2048 pixels, 10 µm pixel size, and 35,000 Hz line rate. The camera was connected to the laptop computer by a PCMCIA data acquisition card which supported a camera-link interface (VCE CLCB01, Imperx).

LCI PROBE: The LCI probe was custom-designed with a small diameter (0.5 - 0.7 mm) and a long working distance (12-14 mm) to match the video otoscope optics. A gradient index (GRIN) lens with a diameter of 0.5 mm, length of ~3.5 mm, and working distance of 6 mm was initially used. The 8° polish angles of the lens prevented large back

#132874 - $15.00 USD Received 4 Aug 2010; revised 4 Oct 2010; accepted 4 Oct 2010; published 7 Oct 2010

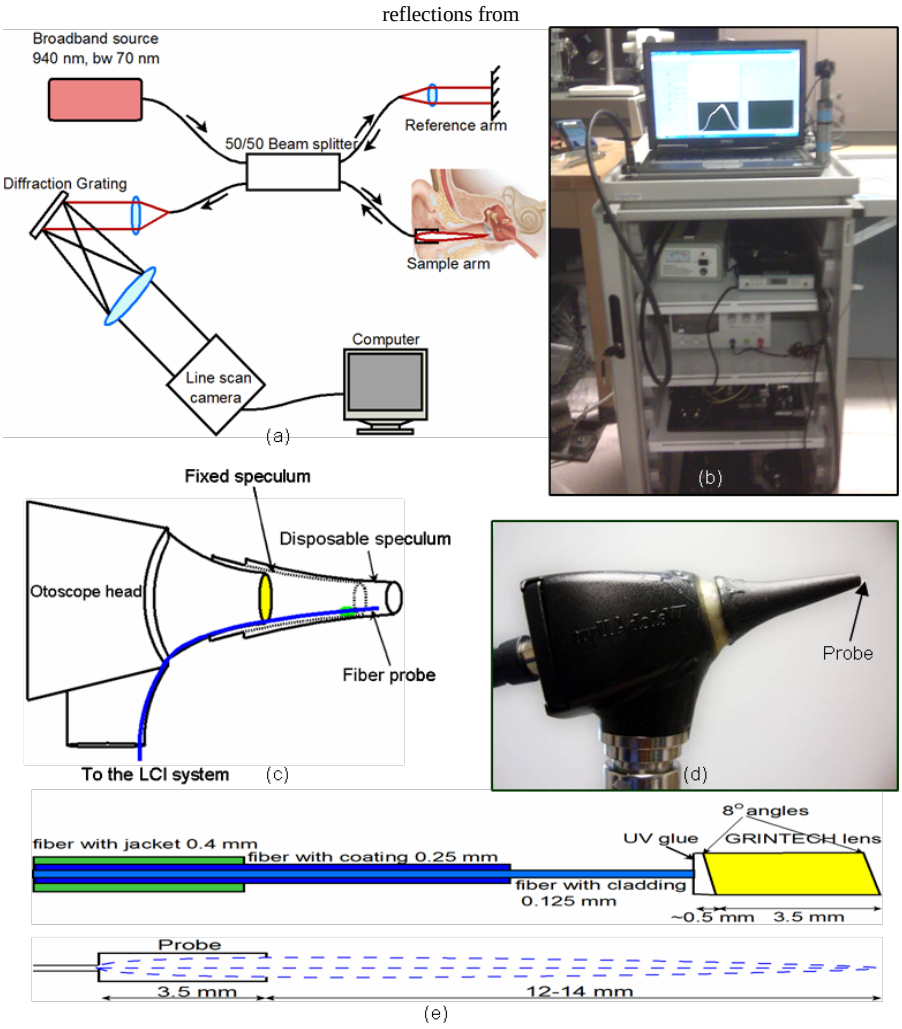

Fig. 1. Portable LCI otoscope system. (a) Diagram and (b) photograph of the portable system. (c,d) Integration of the LCI fiber-based micro-optic probe into the otoscope head. (e) Schematic and beam profile of the long working distance LCI probe.

surfaces of the probe. In order to achieve the long working distance, this lens was then polished and glued to the fiber. The polished length of the lens and the glue layer thickness were calculated by theory and simulation in a related study [24]. The final probes had a long working distance in the range of 12-14 mm and a spot size of ~30 µm (transverse resolution). The focused beam profile is shown schematically in Fig. 1(e).

The distal end of this fiber probe was positioned within a plastic ear speculum tip to enable the focused spot to be located within the field of view of the video otoscope image [Figs. 1(c) and 1(d)]. A standard video otoscope (Model 23120, Welch Allyn, Inc.) was used for these studies so that the real-time otoscope CCD-camera video could be used to track the location of the LCI beam, as well as provide digital video imaging of the TM surface illuminated with white-light from the otoscope illumination source. This LCI system could also readily interface with other standard (non-video) otoscopes as well, provided that an additional visible aiming beam was co-linearly propagated with the LCI beam and incident on the TM.

#132874 - $15.00 USD Received 4 Aug 2010; revised 4 Oct 2010; accepted 4 Oct 2010; published 7 Oct 2010

The physician uses the system in a manner similar to a digital video otoscope. Real-time video images presented in the software user interface enable the guidance of the LCI beam. While the 940 nm LCI beam is outside the range for human visual perception, the beam can be visualized in the video images by a bright spot, as the silicon-based CCD cameras are sensitive out to nearly 1100 nm. The functions of the program such as data acquisition, review, storage, and analysis are all designed to be user friendly.

2.3. Classification algorithm

Three parameters were extracted from each LCI scan to serve as inputs to the classification algorithm. These parameters are thickness of the TM with or without a biofilm layer, intensity of optical backscatter, and optical attenuation through the TM and any additional structures within the middle ear. The thickness of the TM and biofilm layers is determined by an edge detection algorithm [25,26]. The intensity represents the mean signal over the entire depth scan and the attenuation is defined by the signal slope.

First, thickness and intensity of each LCI axial scan were computed. The thickness was then analyzed to discard superfluous scans and detect the TM region, because during the data collection the probe may be directed to unwanted positions, for example, to the TM region over the malleus or to the edges of the ear canal, where the tissue is much thicker and not representative of the TM.

A normal TM is thinner in the central region and thicker around the periphery. Therefore, LCI data from the central region of normal TMs were detected and differentiated from other data, including data from the periphery of normal TMs and TMs with biofilms or effusion, by a hypothesis detection method based on the thickness and intensity parameters. The typical thickness of the normal TM is 20 μm for rat and 100 μm for human. Biofilm layers increase this thickness by 30-200 μm.

Signal models, based on the thickness, intensity, and attenuation, were generated from the training data and utilized to classify the LCI data. The signal models represented the A-scan characteristics of data groups acquired from the central region of normal TMs, periphery of normal TMs, TMs with early biofilms, TMs with developed biofilms, and TMs with effusion. These groups were formed based on the known structures of TMs [27], biofilms [16], and phantoms for effusions. The mean thickness and intensity were first computed by Bayesian estimation [25,26]. The training data were then normalized to the expectation value of the thickness and intensity. The model was the average of these normalized training data.

Next, a minimum distance classification was implemented on pre-processed data [25,26]. The pre-processing steps normalize the thickness and intensity of the input signal to enable pattern matching with the models. The best match model minimized the Euclidean distance between the given model and input data (Fig. 2).

From the result of axial scan classification, data from normal TMs at both the central and peripheral regions were considered as normal axial scans. Other data types from TMs with biofilms or effusion were considered as abnormal axial scans. Percentages of normal and abnormal axial scans from the total acquired axial scans were then used to determine the probability of a biofilm with or without an effusion. This quantitative data on the thickness of TMs, type and thickness of biofilm, and the presence and type of effusion could also be helpful for OM diagnosis.

#132874 - $15.00 USD Received 4 Aug 2010; revised 4 Oct 2010; accepted 4 Oct 2010; published 7 Oct 2010

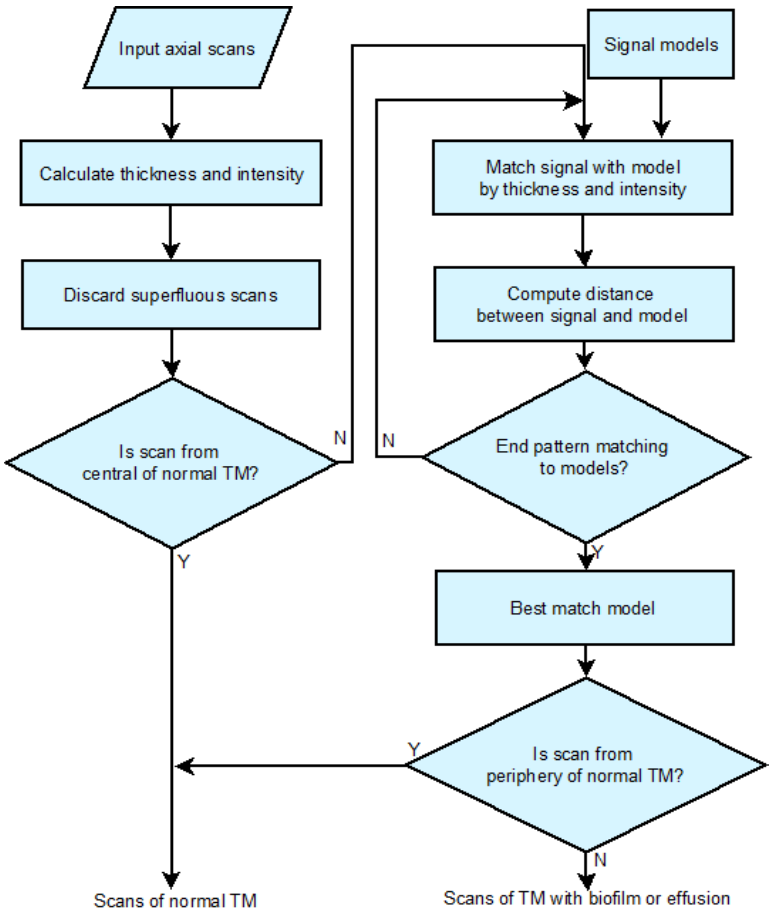

Fig. 2. Signal processing flow-chart for the axial scan classification algorithm.

3. Results

During the 7 month animal study, 8 animals were inoculated. One animal that was not inoculated served as a control. Noticeable changes were observed in the TMs of the inoculated rats compared to the control animal using both the otoscopy images and LCI data, even though most inoculated animals did not appear sick during the inoculation period. TMs of all inoculated animals were monitored in every inoculation session. Otoscopy images and LCI data were captured if any pathological change were found in TMs by standard otoscopy. *Ex vivo* OCT and histology images of TMs were also acquired if the rat appeared severely infected, based on data obtained by otoscopy and LCI.

The first acute OM was noticed by otoscopy after 7 weeks of inoculations. The TMs of this animal had darker and branching vessels, and half of one TM appeared red and cloudy. Several acute OMs were also recorded in 3 animals in both groups of rats. However, these OMs cleared quickly in 2-3 days. Histological observations from one TM from a rat with acute OM confirmed the presence of bacterial colonization behind the TM. The most interesting result was found in one animal in the second group. A severe infection was observed after 4 months of inoculations, and following two recorded episodes of acute OM. The TM from this animal was dark red, prominent, and damaged with two perforations. Data from the middle ear of this rat acquired by LCI, OCT, and histology also confirmed the severe infection and the presence of additional structures behind the TM.

#132874 - $15.00 USD Received 4 Aug 2010; revised 4 Oct 2010; accepted 4 Oct 2010; published 7 Oct 2010

The TM of the normal rat appeared translucent by video otoscopy [Fig. 3(a)] and the corresponding typical LCI signal showed a single thin structure representing the thin TM [Fig. 3(b)]. This thin TM was also confirmed in the corresponding OCT and histology images from the same rat [Figs. 3(c) and 3(d)]. The OCT images of the dissected TM were acquired with the OCT beam incident on the inner surface of the TM, rather than on the external surface, in order to provide a full field-of-view. The narrow external ear canal of the rat prohibited OCT imaging across the full width of the TM from this orientation. Major portions of the TM were thin, while the periphery of the TM was noticeably thicker.

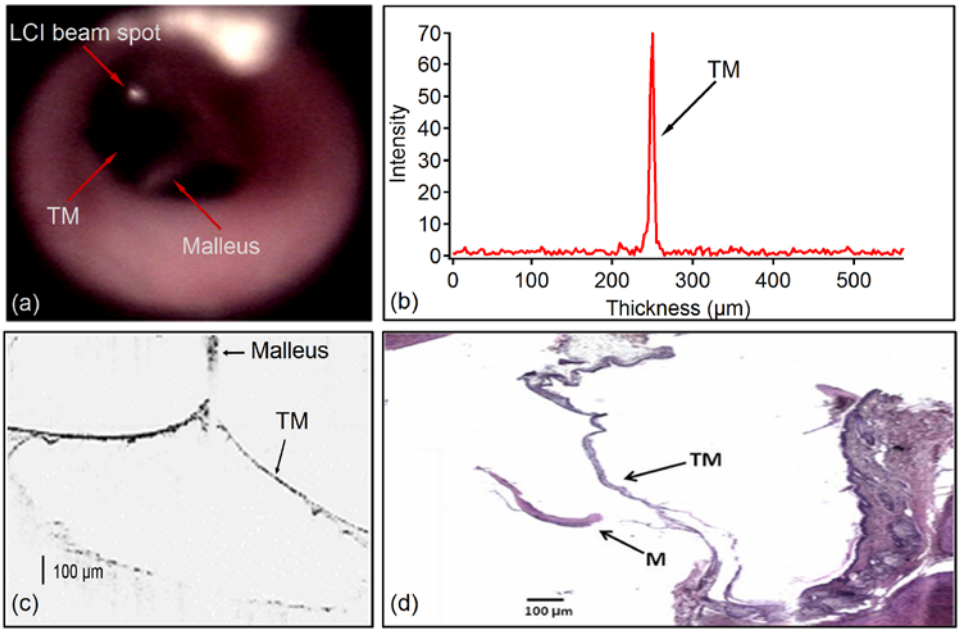

Fig. 3. Typical *in vivo* data of normal rat TM acquired with LCI otoscope system. (a) Video image of middle ear. (b) LCI axial scan of TM. (c) Validation data from 2-D OCT image acquired *ex vivo*. (d) Corresponding histology (M, Malleus). The thin membrane is representative of the TMs from normal rats.

In contrast, video otoscopy from the infected TM appeared cloudy, dark red, and with prominent perforated regions [Fig. 4(a)]. The LCI signals from the infected rat TM exhibited additional scattering structures behind the TM. As an example, in the typical LCI scan, the additional structure appeared thick and lower scattering immediately adjacent to the thin and higher scattering TM. This structure was ~120 μm thick, six times thicker than the TM from a normal rat [Fig. 4(b)]. In the *ex vivo* OCT images from the middle ear of the infected rat, the additional structure behind the TM was confirmed. The presence of the two prominent regions with perforations filled by blood was also shown in the OCT images [Fig. 4(c)]. These findings from the infected TM were apparent in the histological images as well. Even though some portions of the biofilm were not seen in the histological images (likely due to processing artifacts) as in the OCT images, the left portion of the biofilm (blue arrows), the two perforations (red squares), and bacterial colonies (blues square) [Fig. 4(d)] were evident, which validated the presence of a bacterial biofilm as detected in the LCI data.

#132874 - $15.00 USD Received 4 Aug 2010; revised 4 Oct 2010; accepted 4 Oct 2010; published 7 Oct 2010

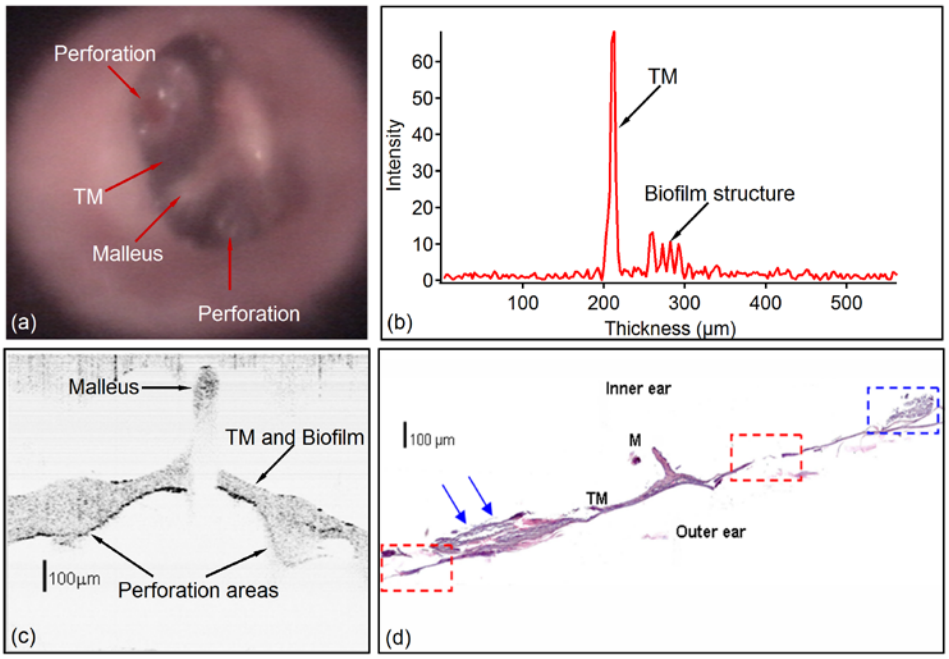

Fig. 4. Typical *in vivo* data of infected rat TM acquired with LCI otoscope system. (a) Video image of middle ear. (b) LCI axial scan of TM. (c) Validation data from 2-D OCT image acquired *ex vivo*. (d) Corresponding histology. Note the increased thickness of the TM and biofilm structures in LCI, OCT, and histology images (blue arrows). The prominent areas with TM perforations filled by blood, as seen in (a), are also recognized in OCT and histology (red squares).

The *in vivo* video images of the rat TM are out-of-focus because the very narrow ear canals prevented full insertion of the human otoscope ear speculum tip. To enable LCI data collection within the small rat ear canal, a bare LCI probe tip was inserted directly, and real-time LCI signals were used to monitor the position and placement where *in vivo* LCI data were collected, relative to the TM. By this method, 74 *in vivo* axial scans were successfully acquired. Despite this relatively limited number of LCI scans, there was a sufficient number to show the presence of additional scattering structures behind the TM, which were indicative of a biofilm.

The classification algorithm was applied to both *in vivo* and *ex vivo* LCI data. The *ex vivo* LCI data was extracted from the 2-D OCT images acquired at positions that uniformly sampled the full area of the TM, including undesired areas such as areas overlying the malleus, and regions at the periphery of the TM. The axial scans from these undesired regions over the malleus or peripheral skin regions showed a thickness of ~200-300 μm, compared to 20-150 μm from the rat TM, with or without a biofilm. Therefore, these scans from undesired regions were automatically eliminated by thickness classification.

Figure 5(a) reports the classification of the LCI data for *ex vivo* OCT data based on the thickness and intensity of the filtered axial scans. There is clear separation between scans classified as normal from the control rat (blue circles) and those classified as infected from the infected rat (red circles). Some data points from the infected rat (left red circles) fell within the normal area because they came from regions of the TM that did not have biofilms, as confirmed by histology. Similarly, some data points from normal TMs (right blue circles) fell within the area classified as infected. These data points correspond to LCI scans acquired from regions over the malleus and around the periphery of the TM, where natural thickening occurs.

#132874 - $15.00 USD Received 4 Aug 2010; revised 4 Oct 2010; accepted 4 Oct 2010; published 7 Oct 2010

The model classification was then applied to classify the filtered *ex vivo* LCI data into defined categories. From 1,786 axial scans from normal rats, 1,561 scans were classified as normal types (blue circles) and 225 axial scans were classified as abnormal types (blue crosses). The majority of scans from the normal rats were classified as a normal thin TM. From 1,597 axial scans from infected rats, 167 axial scans were classified as normal types (red crosses) and 1,430 axial scans were classified as abnormal types (red circles) [Fig. 5(b)]. The majority of scans from the infected rats were classified as a TM with an established biofilm. The sensitivity and specificity of LCI with this classification algorithm for detecting the presence of a biofilm were 87% and 90%, respectively, using histological findings as the gold standard.

Since the *in vivo* LCI data were acquired without video guidance, the sensitivity and specificity of *in vivo* LCI data classification were significantly lower (78% and 83%, respectively). Figures 5(c) and 5(d) indicate that a larger portion of data was acquired from the peripheral regions of the TMs in the normal rats and from the thin regions of the TM in the infected rat. These data increase the false positive and false negative cases and, hence, decrease the sensitivity and specificity.

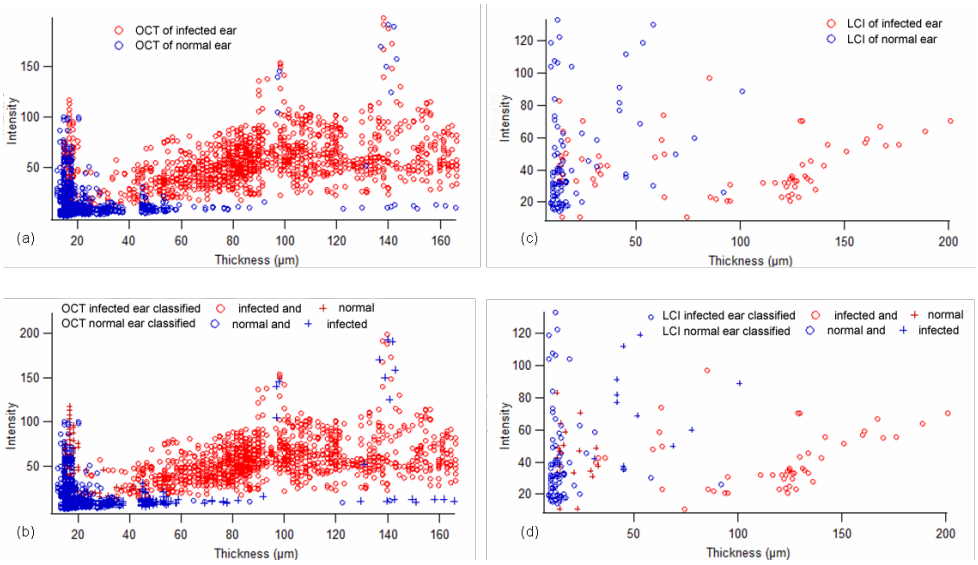

Fig. 5. Acquired and classified axial scan data represented by thickness and intensity. Acquired (a) *ex vivo* OCT data and (c) *in vivo* LCI data. Classified (b) *ex vivo* OCT data and (d) *in vivo* LCI data, the cross symbols represent the misclassified axial scans.

4. Discussion

Diagnosing chronic OM is a challenge. Normally, chronic OM does not have signs that can be easily recognized by otoscopy, as with acute OM. Three popular methods have been used to diagnose chronic OM: standard otoscopy, pneumatic otoscopy, and tympanometry. However, the accuracy of these methods is limited. Therefore, a combination of these methods is currently used for chronic OM diagnosis in order to achieve higher sensitivity and specificity. Besides the accuracy of diagnosis, quantitative characterization of acute or chronic OM is also limited using the available methods. Thus, a new diagnostic tool for middle ear infections which could overcome the discussed limitations is highly motivated. Our work has presented a novel diagnostic method for middle ear infections using low-coherence interferometry that is able to detect, quantify, and monitor middle ear biofilms non-invasively. A new animal biofilm model has also been developed and used for validating our method.

#132874 - $15.00 USD Received 4 Aug 2010; revised 4 Oct 2010; accepted 4 Oct 2010; published 7 Oct 2010

An enhanced otoscopy system has been constructed and its application demonstrated by collecting LCI and video otoscopy data from this rat middle ear biofilm model. This portable system has a depth resolution of ~4.5 μm, an imaging depth range of ~2 mm, and thus is appropriate for readily accessing the TM and assessing the presence of biofilms on the inner surface, as well as the presence of any middle ear effusion. The observable differences between the LCI signals from normal and infected rat TMs demonstrate the capability and sensitivity for detecting middle ear biofilms. These new data offer the possibility to classify OM status, to observe and more accurately quantify the association of middle ear biofilm growth with the progression of acute OM to chronic OM, and ultimately provide quantitative data to direct appropriate therapies.

Since the rat TM and middle ear structures are similar to those in the human ear (with human structures larger in scale), the positive results from this pre-clinical animal study demonstrate the potential use of this enhanced otoscopy system for research and clinical use for the diagnosis, quantification, and monitoring of human OM. With the current system, axial scans are collected continuously in time and randomly in space, guided by both real-time video otoscopy and real-time LCI data collection. The collection of a large number of axial scans is sufficient to adequately sample the TM regions and classify the scans. Further miniaturization and use of MEMs-based scanners [17,18] would enable the rapid acquisition of 2-D and 3-D OCT images, but with increased equipment cost, equipment complexity, and longer computational processing and analysis time.

In addition to the novelty of this enhanced otoscopy system and technique, this study represents the first demonstration of biofilm induction and growth by nostral inoculation and pressurization in rats. Typically, OM is induced via puncture of the TM, and only recently OM has been induced via nostril inoculation. At the time of this study, there had been no such animal model for inducing and growing biofilms. Though our rat model had been successfully applied for inducing OM and growing biofilms, it was also found to be a challenging model for imaging, especially for *in vivo* OCT, due to the narrow external ear canal. The immune system of these rats also proved to be robust against OM. Though OM infections were frequently observed for 1-2 days after each inoculation, the infection appeared to be readily cleared, despite regular bi-weekly inoculations. Seven of eight inoculated rats did not show biofilms despite a long inoculation period and recurrent infections. However, it should be noted that this pattern of infection and clearance is not completely unlike the process in humans, which is believed to lead to the formation of biofilms over time [7]. As noted, the rat outer ear canal is very narrow, prompting the development of long working distance probes, and frequently out-of-focus video otoscopy images, resulting in limited video guidance to TM locations. Based on these study results, other animal models such as the chinchilla [23] will be investigated for future *in vivo* biofilm growth and antibiotic response studies.

The noted limitations of out-of-focus video otoscopy and reduced visual guidance of LCI beam placement experienced during this animal study are likely to be fully resolved during studies in humans. Since the standard otoscope and specula used in this study were designed for use in the human ear, which is much larger than the rat ear, the LCI otoscope will have both video images and the LCI probe beam in focus. Real-time otoscopy video as well as real-time LCI data acquisition would be used to guide the LCI probe beam to areas of interest across the TM. The real-time guidance would not only lead to the collection of an adequate number of axial scans but will also improve the efficiency of the classification by guiding the probe to the most pathologically suspicious areas that can be observed by the video.

The classification algorithm developed during this research has proved to be highly effective for classifying LCI data from normal and infected TMs. The results of 86% sensitivity and 90% specificity, compared to histological findings, are higher than those for the diagnosis of chronic OM (74% and 60%) using standard otoscopy. Other currently available diagnostic methods such as pneumatic otoscopy and tympanometry can yield slightly higher sensitivities and specificities (70-90%) compared to standard otoscopy, but

#132874 - $15.00 USD Received 4 Aug 2010; revised 4 Oct 2010; accepted 4 Oct 2010; published 7 Oct 2010

these methods depend heavily on patient cooperation [5]. We expect to achieve the same or better sensitivity and specificity for *in vivo* human LCI data classification, compared to what was achieved in this study with rat LCI data classification. In human studies, thousands of LCI axial scans will be acquired within 5-10 seconds under video-guidance, which will be used for classification. This rapid collection of LCI data is expected to be less dependent on patient cooperation than one measurement using pneumatic otoscopy or tympanometry, which commonly requires 10-30 seconds. Directing the LCI probe to the areas on the TM which are highly suspicious under otoscopy observations should also yield an expected improvement in sensitivity and specificity since fewer scans would be collected from regions that would not contain biofilms, such as over the malleus or from the epithelial tissue regions around the periphery of the TM. Since video otoscopy images are captured simultaneously as the LCI depth-scan data, and since the location of the LCI beam on the TM can be visualized on the video images, it is possible to use computer image processing methods to automatically determine which LCI scans were not from the TM, and discard these data prior to classification. The variety of clinical pathologies and additional training data collected over time are expected to further enhance the characteristics of the signal models and subsequently further improve the sensitivity and specificity of the classification algorithm.

Otitis media is one of the most common diseases in children. Detecting chronic OM and tracking antibiotic responses are the major challenges for the diagnosis and treatment of OM. Based on the correspondence between chronic OM and the presence of a bacterial biofilm behind the TM, we were able to diagnose chronic OM by detecting bacterial biofilms in the middle ear. To summarize, using an enhanced portable otoscopy system we demonstrated the application of LCI/OCT for OM diagnosis and the detection, classification, and quantification of middle ear biofilms in a new animal model for this disease. LCI signals with high axial resolution were selected to classify TMs and additional structures like biofilms and effusions related to chronic OM. The real-time data, assessment, and classification captured in an office-based clinical setting have the potential for assisting in the management of chronic OM.

Acknowledgments

We thank Dr. Michael Novak from the Department of Otolaryngology, Carle Physicians Group, Urbana, Illinois, for his clinical input and insight related to this work. This work was supported in part by Blue Highway, LLC, Welch Allyn, Inc., and the National Institutes of Health (NIBIB R01 EB005221). Additional information can be found at http://biophotonics.illinois.edu.

#132874 - $15.00 USD Received 4 Aug 2010; revised 4 Oct 2010; accepted 4 Oct 2010; published 7 Oct 2010